RESTORATION OF MULTILAYERED SINGLE-PHOTON 3D LIDAR IMAGES

Abderrahim Halimi, Rachael Tobin, Aongus McCarthy, Stephen McLaughlin, Gerald S. Buller

School of Engineering and Physical Sciences, Heriot-Watt University, Edinburgh U.K.

ABSTRACT

This paper presents a new algorithm for the restoration of multilayered three-dimensional laser detection and ranging (3D Lidar) images. For multilayered targets such as semi-transparent surfaces or when the transmitted light of the laser beam is incident on multiple surfaces at different depths, the returned signal may contain multiple peaks. Considering the Poisson statistics of these observations leads to a convex data fidelity term that is regularized using appropriate functions accounting for the spatial correlation between pixels and the sparse depth repartition of targets. More precisely, the spatial correlation is introduced using a convex total variation (TV) regularizer, and a collaborative sparse prior is used to introduce the depth prior knowledge. The resulting minimization problem is solved using the alternating direction method of multipliers (ADMM) that offers good convergence properties. The algorithm was validated using field data representing a man standing 1 meter behind camouflage, at an approximate stand-off distance of 230m from the system. The results show the benefit of the proposed strategy in that it improves the quality of the imaged objects at different depths and under reduced acquisition times.

Index Terms— Lidar waveform, Poisson statistics, image restoration, ADMM, total variation, collaborative sparsity.

1. INTRODUCTION

The time-of-flight (ToF) laser detection and ranging (Lidar) system can be used to reconstruct three-dimensional scenes by emitting laser pulses and recording the reflected signal from the target [1]. By using the time-correlated single-photon counting (TCSPC) module (HydraHarp 400, PicoQuant), a photon number histogram can be compiled for each pixel with respect to (w.r.t.) each photon time-of-flight [2]. When the observed scene contains semi-transparent surfaces or the laser beam covers many depth surfaces, the obtained histogram may contain multiple peaks, due to the multi-layered target. In this case, the time delay and the amplitude of the histogram peaks are related to the distances and reflectivities of the observed objects, respectively, which allows for the reconstruction of the 3D scene.

This paper considers the reconstruction and restoration of 3D multi-layered scenes constructed using the single-photon approach, which has a limited shot-noise sensitivity, and a fine surface-to-surface resolution that can be of millimeter scale even at long distances. A similar problem has already been considered in [3] which used a Bayesian formulation solved using a Markov chain Monte-Carlo (MCMC) algorithm. The resulting algorithm shows promising results, however, MCMC algorithms are known to be time-consuming which prevent their use in practical situations. Another algorithm has recently been proposed in [4] by considering a convex formulation coupled with an ℓ_1 sparsity promoting regularizer. This approach takes into account the Poisson statistics of the data and assumes the sparsity of the received photons. However, it does not account for the target continuity of surfaces and may lead to the detection of background noise as a target.

This work proposes a solution to these issues by considering a relatively fast algorithm (w.r.t. MCMC) that reconstructs 3D scenes while taking into account prior knowledge about the observed targets. Target reconstruction is obtained by minimizing a convex function composed of a data fidelity and regularization terms. The former is built based on the Poisson distribution of the observed photon counts and using a linear formulation similar to that proposed in [4]. Regarding the regularization terms, we first assume the presence of spatial correlation for each observed object, which is introduced using a convex total variation (TV) regularizer [5]. Thanks to the fine depth resolution and the large observed range window, we also assume that the number of layers is lower than the number of available time bins, which is introduced using a collaborative sparse prior (group-sparsity) [6–8]. The resulting optimization problem is then solved by developing a new variant of the alternating direction method of multipliers (ADMM) algorithm [9–12]. The results obtained using field data representing a man standing 1 meter behind camouflage, at an approximate distance of 230m, shows the benefit of the proposed strategy in that it improves the quality of the image even when reducing the acquisition time.

The paper is structured as follows. Section 2 describes the observation model associated with the photon counts. The proposed formulation for regularized problem and the estimation algorithm are presented in Section 3. Section 4 presents

This work was supported by the UK Defence Science and Technology Laboratory (DSTL) and EPSRC Grants EP/J015180/1, EP/N003446/1, EP/M01326X/1, EP/K015338/1.

ISBN 978-0-9928626-7-1

simulation results obtained using actual time-of-flight scanning sensor data. Conclusions and future work are finally reported in Section 5.

2. OBSERVATION MODEL

The Lidar observation $\boldsymbol{y}_{n,t}$, where $n \in \{1, \cdots, N\}$, represents the number of photon counts within the tth bin of the nth pixel. When the observed scene contains semi-transparent surfaces or the laser beam covers many depth surfaces, the returned signal may contain multiple peaks, located at distances related to the observed depths. The observed photon counts $\boldsymbol{y}_{n,t}$ are distributed according to a Poisson distribution $\mathcal{P}(.)$ as follows [13, 14]

$$y_{n,t} \sim \mathcal{P}(s_{n,t}) \tag{1}$$

where

$$s_{n,t} = \sum_{m=1}^{M_n} [r_{n,m} g_0(t - k_{n,m}T)] + b_n \tag{2}$$

and M_n is the number of layers in the nth pixel, T is the time resolution of the system, $k_{n,m} \geq 0$ is the range's position of the mth object from the sensor (related to its depth), $r_{n,m} \geq 0$ is the mth reflectivity of the target, $b_n \geq 0$ denotes the background and dark counts of the detector, and g_0 represents the system impulse response (SIR) assumed to be known from the calibration step. The discrete time version of (2), when considering K time bins, can be expressed as a linear system (convolution by the SIR) as follows [4]

$$\boldsymbol{s}_n = \boldsymbol{G}\boldsymbol{x}_n \tag{3}$$

where $\boldsymbol{G} = [\boldsymbol{g}_1, \cdots, \boldsymbol{g}_K, \boldsymbol{1}_{K\times 1}]$ is a $K\times(K+1)$ matrix gathering shifted impulse responses, $\boldsymbol{1}_{i\times j}$ denotes the $(i \times j)$ matrix of 1, $\boldsymbol{g}_i = [g_0(T-iT), g_0(2T-iT), \cdots, g_0(KT-iT)]^\top$ is a $(K \times 1)$ vector representing the discrete impulse response centered at iT and $\boldsymbol{x}_n$ is a $(K+1) \times 1$ vector whose value are zero except for $\boldsymbol{x}_n(k_{n,m}) = r_{n,m}, \forall m$, and $\boldsymbol{x}_n(K+1) = b_n$. Using (3), straightforward computations show that the negative-log-likelihood associated with the discrete observations $\boldsymbol{y}_{n,k} \sim \mathcal{P}[(\boldsymbol{G}\boldsymbol{x}_n)_k]$ is given by

$$\mathcal{L}_n(\boldsymbol{x}_n) = \mathcal{H}_n(\boldsymbol{G}\boldsymbol{x}_n) \tag{4}$$

where $\mathcal{H}_n : \mathbb{R}^K_{>0} \to \mathbb{R}\{-\infty, +\infty\}$ is given by

$$\mathcal{H}_n(\boldsymbol{z}) = \sum_{k=1}^{K} z_k - \boldsymbol{y}_{n,k} \log(z_k). \tag{5}$$

Finally, assuming independence between the observed pixels leads to the following negative-log of the joint likelihood

$$\mathcal{L}(\boldsymbol{X}) = -\log[P(\boldsymbol{Y}|\boldsymbol{X})] = \sum_n \mathcal{L}_n(\boldsymbol{x}_n) \tag{6}$$

where $\boldsymbol{Y}$ (resp. $\boldsymbol{X}$) is a $K \times N$ (resp. $(K+1) \times N$) matrix gathering the vectors $\boldsymbol{y}_n$ (resp. $\boldsymbol{x}_n$). The goal is then to estimate the sparse matrix $\boldsymbol{X}$, where the positions and values of the non-zero elements correspond to the target depths and intensities, respectively.

3. THE ESTIMATION ALGORITHM

3.1. Regularized problem

This section introduces the proposed regularized problem to estimate the matrix $\boldsymbol{X}$. To this end, we adopt an optimization approach that minimizes a regularized data fidelity cost function. More precisely, considering the data Poisson statistics lead to the data fidelity term $\mathcal{L}(\boldsymbol{X})$ presented in (6). Estimating the matrix $\boldsymbol{X}$ is an ill-posed inverse problem that requires the introduction of prior knowledge (or regularization terms) related to the target depths and reflectivities. In this paper we consider two assumptions: (i) the observed objects present spatial correlations; (ii) a small number of depths are active with respect to the observation range window. With these considerations in mind, we propose to solve the following optimization problem

$$\mathcal{C}(\boldsymbol{X}) = \mathcal{L}(\boldsymbol{X}) + i_{\mathbb{R}_+}(\boldsymbol{X}) + \tau_1 ||\boldsymbol{W}\boldsymbol{X}||_1 + \tau_2 ||\boldsymbol{X}||_{2,1} \tag{7}$$

where $\boldsymbol{W} = \boldsymbol{D}\boldsymbol{H}\boldsymbol{G}$ represent a linear operator whose components are explained later in the text, $\tau_1 > 0$, $\tau_2 > 0$ are two regularization parameters, and $i_{\mathbb{R}_+}(\boldsymbol{X}) = \sum_{n,k} i_{\mathbb{R}_+}(x_{n,k})$ is the indicator function that imposes positivity ($i_{\mathbb{R}_+}(m) = 0$ if m belongs to the non-negative orthant and $+\infty$ otherwise). The first two terms of (7) are the data fidelity term associated with the Poisson statistics and a convex term imposing positivity on $\boldsymbol{X}$. The other terms of (7) account for the prior knowledge of $\boldsymbol{X}$. The convex term $||\boldsymbol{W}\boldsymbol{X}||_1$ is an ℓ_1 norm that promotes element-wise sparsity on the projected matrix $\boldsymbol{W}\boldsymbol{X}$. This projection matrix should be carefully chosen to promote the desired spatial correlation. Because of the fine depth resolution, a large number of time bins is used in the histograms leading to sparse photon counts in each time bin at each pixel of the observed data $\boldsymbol{Y}$, especially when reducing the acquisition time. This effect may deteriorate the performance of the considered spatial regularization. To solve this issue, a TV spatial regularization is applied to the convolved signal $\boldsymbol{X}$ (by the SIR) after summing the counts inside a window of ranges with predefined width $\#h$. This prevents the sparse spatial repartition of the photons and improves the performance of the TV operator. For a formal mathematical description, the procedure is achieved using $\boldsymbol{W} = \boldsymbol{D}\boldsymbol{H}\boldsymbol{G}$, with $\boldsymbol{D}$ the linear TV operator [12], and $\boldsymbol{H} = \mathbb{I} \otimes \boldsymbol{1}_{1\times h}$, is a matrix summing the photon counts of each $\#h$ successive time bins of the convolved signal $\boldsymbol{G}\boldsymbol{X}$, where $\otimes$ denotes the Kronecker product and $\mathbb{I}$ the identity matrix of adequate size. The convex term $||\boldsymbol{X}||_{2,1} = \sum_{k=1}^{K} ||\boldsymbol{x}_k||_2 = \sum_{k=1}^{K} \sqrt{\boldsymbol{x}_k^T \boldsymbol{x}_k}$ is the ℓ_{21} mixed norm of $\boldsymbol{X}$ which promotes sparsity among the columns of $\boldsymbol{X}$, that is, the solutions of (7) are encouraged to have a small number of active depths. This term is called collaborative regularization since it promotes group-sparsity over the columns of $\boldsymbol{X}$ by using the information in all the pixels. It has recently received increasing interest by the image processing community as illustrated in [6–8]. The proposed

ISBN 978-0-9928626-7-1

formulation in (7) combines the ℓ_{21} mixed norm with the ℓ_1 norm which leads to a slightly different effect, i.e., it allows for sparsity under a dictionary inside the active columns of $\boldsymbol{X}$. The resulting sum of convex functions (7) can be solved using different algorithms such as the ADMM algorithm [9] or primal-dual algorithms [15]. In this paper, we use the ADMM algorithm that is described in the next section [9, 10, 16].

3.2. The ADMM algorithm

Consider the optimization problem

$$\underset{\boldsymbol{X},\boldsymbol{V}}{\text{argmin}}\, g\left(\boldsymbol{V}\right), \text{subject to } \boldsymbol{A}\boldsymbol{X}+\boldsymbol{B}\boldsymbol{V}=0 \tag{8}$$

where $\boldsymbol{X} \in \mathbb{R}^{(K+1)\times N}$, $g(.)$ is a closed, proper, convex function, and $\boldsymbol{A}$, $\boldsymbol{B}$ are arbitrary matrices. The ADMM algorithm consists first in computing the augmented Lagrangian for problem (8), as follows

$$\mathcal{AL}\left(\boldsymbol{X},\boldsymbol{V},\boldsymbol{F}\right)=g\left(\boldsymbol{V}\right)+\frac{\mu}{2}||\boldsymbol{A}\boldsymbol{X}+\boldsymbol{B}\boldsymbol{V}-\boldsymbol{F}||_F^2 \tag{9}$$

where μ is a positive constant, and $\boldsymbol{F}/\mu$ denotes the Lagrange multipliers associated with the constraint $\boldsymbol{A}\boldsymbol{X}+\boldsymbol{B}\boldsymbol{V}=0$. As a second step, the algorithm optimizes $\mathcal{AL}$ sequentially with respect to $\boldsymbol{X}$ and $\boldsymbol{V}$, and then updates the Lagrange multipliers as shown in Algo. 1.

Algorithm 1 ADMM for (8)

1: Initialization
2: Initialize $\boldsymbol{X}_j^{(0)}, \boldsymbol{V}_j^{(0)}, \boldsymbol{F}_j^{(0)}, \forall j, \mu > 0$.
3: Set $i \leftarrow 0$, conv$\leftarrow 0$
4: **while** conv$= 0$ **do**
5: $\quad \boldsymbol{X}^{(i+1)} \leftarrow \underset{\boldsymbol{X}}{\text{argmin}}\, \mathcal{AL}\left(\boldsymbol{X}, \boldsymbol{V}^{(i)}, \boldsymbol{F}^{(i)}\right)$
6: $\quad \boldsymbol{V}^{(i+1)} \leftarrow \underset{\boldsymbol{V}}{\text{argmin}}\, \mathcal{AL}\left(\boldsymbol{X}^{(i+1)}, \boldsymbol{V}, \boldsymbol{F}^{(i)}\right)$
7: $\quad \boldsymbol{F}^{(i+1)} \leftarrow \boldsymbol{F}^{(i)} - \boldsymbol{A}\boldsymbol{X}^{(i+1)} - \boldsymbol{B}\boldsymbol{V}^{(i+1)}$
8: $\quad$ conv$\leftarrow 1$, if the stopping criterion is satisfied.
9: **end while**

Algo. 1 converges when the function g is closed, proper, and convex and $\boldsymbol{A}$ is full column rank [17, Theorem 1]. The latter theorem also states that the sequence $\boldsymbol{X}^{(i)}$ converges to a solution of (8), for any $\mu > 0$, if it has a non-empty set of solutions. If (8) does not have a solution, then at least one of the sequences $\boldsymbol{X}^{(i)}$ or $\boldsymbol{F}^{(i)}$ diverges. Note that the details of the steps of Algo. 1 are not provided for brevity, however, they reduce to the solution of a linear system of equations (line 5), the computation of Moreau proximity operators [18] (line 6), and the updating of the Lagrange multipliers (line 7). The convergence speed of the algorithm is affected by the parameter μ, that has been updated using the adaptive procedure described in [8, 9]. This procedure keeps the ratio between the ADMM primal and dual residual norms within a given positive interval, as they both converge to zero. The algorithm is stopped when these residual norms are lower than a given threshold [9]. Note finally that more details regarding the ADMM algorithm are available in [8–10, 16] for the interested reader.

3.3. Proposed algorithm

This section presents the optimization problem considered for estimating the matrix of interest $\boldsymbol{X}$. Using the same notation as in (8), problem (7) can be expressed as follows

$$g\left(\boldsymbol{V}\right)=\mathcal{H}\left(\boldsymbol{V}_1\right)+i_{\mathbb{R}_+}\left(\boldsymbol{V}_2\right)+\tau_1||\boldsymbol{V}_4||_1+\tau_2||\boldsymbol{V}_5||_{2,1} \tag{10}$$

with $\boldsymbol{V}_1=\boldsymbol{G}\boldsymbol{X}$, $\boldsymbol{V}_2=\boldsymbol{X}$, $\boldsymbol{V}_3=\boldsymbol{H}\boldsymbol{G}\boldsymbol{X}$, $\boldsymbol{V}_4=\boldsymbol{D}\boldsymbol{V}_3$, $\boldsymbol{V}_5=[\mathbb{I}_K,\boldsymbol{0}]\boldsymbol{X}$ leading to $\boldsymbol{A}=[\boldsymbol{G},\mathbb{I}_{K+1},\boldsymbol{H}\boldsymbol{G},\boldsymbol{0},(\mathbb{I}_K,\boldsymbol{0})]^\top$ and

$$\boldsymbol{B}=\begin{bmatrix} -\mathbb{I}_{K+1} & \boldsymbol{0} & \boldsymbol{0} & \boldsymbol{0} & \boldsymbol{0} \\ \boldsymbol{0} & -\mathbb{I}_{K+1} & \boldsymbol{0} & \boldsymbol{0} & \boldsymbol{0} \\ \boldsymbol{0} & \boldsymbol{0} & -\mathbb{I}_K & \boldsymbol{0} & \boldsymbol{0} \\ \boldsymbol{0} & \boldsymbol{0} & \boldsymbol{D} & -\mathbb{I}_K & \boldsymbol{0} \\ \boldsymbol{0} & \boldsymbol{0} & \boldsymbol{0} & \boldsymbol{0} & -\mathbb{I}_K \end{bmatrix}. \tag{11}$$

where $\mathbb{I}_n$ denotes the $n \times n$ identity matrix, and $\boldsymbol{0}$ denotes a vector of zeros of adequate size. Note that the constraint $\boldsymbol{V}_4=\boldsymbol{D}\boldsymbol{V}_3$ decouples the optimization in the spatial domain from the optimization in the time (or range) domain which leads to large computational gains, as already suggested in [12]. For this problem, the matrix $\boldsymbol{A}$ is full column rank. This matrix and the properties of $g(.)$ ensure the algorithm convergence. Finally, the optimization problems shown in line 5 and 6 of algo. 1 admit analytical solutions given by (we also invite the reader to consult [11, 12, 19] for more details regarding similar optimization problems)

$$\begin{aligned}
\boldsymbol{X}^{(i+1)} &\leftarrow \left\{\boldsymbol{G}^\top\boldsymbol{G}+\boldsymbol{G}^\top\boldsymbol{H}^\top\boldsymbol{H}\boldsymbol{G}+\begin{bmatrix} 2\mathbb{I}_K & \boldsymbol{0} \\ \boldsymbol{0} & 1 \end{bmatrix}\right\}^{-1} \\
&\quad \times\left\{\boldsymbol{G}^\top\xi_1^{(i)}+\xi_2^{(i)}+\boldsymbol{G}^\top\boldsymbol{H}^\top\xi_3^{(i)}+\begin{bmatrix} \xi_5^{(i)} \\ 0 \end{bmatrix}\right\} \\
\boldsymbol{V}_{1,k,n}^{(i+1)} &\leftarrow \frac{1}{2}\left[z_{k,n}-\frac{1}{\mu}+\sqrt{\left[z_{k,n}-\frac{1}{\mu}\right]^2+4\frac{y_{k,n}}{\mu}}\right] \\
\boldsymbol{V}_2^{(i+1)} &\leftarrow \max\left\{\boldsymbol{X}^{(i)}-\boldsymbol{F}_2^{(i)},0\right\} \\
\boldsymbol{V}_3^{(i+1)} &\leftarrow \left(\boldsymbol{D}^\top\boldsymbol{D}+\mathbb{I}_K\right)^{-1}\left[\boldsymbol{H}\boldsymbol{G}\boldsymbol{X}^{(i)}-\boldsymbol{F}_3^{(i)}+\boldsymbol{D}^\top\xi_4\right] \\
\boldsymbol{V}_4^{(i+1)} &\leftarrow \text{soft}\left(\boldsymbol{F}_4^{(i)}-\boldsymbol{D}\boldsymbol{V}_3^{(i)},\frac{\tau_1}{\mu}\right) \\
\boldsymbol{v}_{5,n}^{(i+1)} &\leftarrow \text{vect-soft}\left(\boldsymbol{F}_{5,n}^{(i)}-(\mathbb{I}_K,\boldsymbol{0})\boldsymbol{x}_n^{(i)},\frac{\tau_2}{\mu}\right),\forall n
\end{aligned} \tag{12}$$

where $\xi_j=\boldsymbol{V}_j^{(i)}+\boldsymbol{F}_j^{(i)}$ for $j\in\{1,2,3,5\}$, $z_{k,n}=\left(\boldsymbol{G}\boldsymbol{x}_n^{(i)}\right)_k-\boldsymbol{F}_{1,k,n}^{(i)}$, $\text{soft}\left(\boldsymbol{X},\frac{\tau}{\mu}\right)=\text{sign}(\boldsymbol{X})\odot\max\left\{|\boldsymbol{X}|-\frac{\tau}{\mu},0\right\}$ denotes the soft threshold operator, $\text{vect-soft}\left(\boldsymbol{x},\frac{\tau}{\mu}\right)=\boldsymbol{x}\left(\frac{\max\left\{||\boldsymbol{x}||_2-\frac{\tau}{\mu},0\right\}}{\max\left\{||\boldsymbol{x}||_2-\frac{\tau}{\mu},0\right\}+\frac{\tau}{\mu}}\right)$ is the vect-soft-threshold operator,

ISBN 978-0-9928626-7-1 © EURASIP 2017

and $|.|$, sign$(.)$, max$(.)$ are the element-wise operators corresponding to the absolute value, the sign function and the maximum operator, respectively.

4. RESULTS ON REAL DATA

The performance of the proposed restoration algorithms are evaluated in this section when considering a real image, composed of 79×40 pixels and 590 time bins, of a man holding a piece of wood standing behind a double layer of camouflage at a stand-off distance of 230m from the system (see Fig. 1). The image was acquired in May 2016 in Virginia, USA, using a time-of-flight scanning sensor, based on the TCSPC technique. The transceiver system and data acquisition hardware used for this work are broadly similar to that described in [20, 21], which uses a 1550nm wavelength and an electrically gated InGaAs/InP single photon avalanche diode (SPAD) detector (see also [14] for more details regarding the system parameters). The image was acquired using a per pixel acquisition time equal to 3.2ms, corresponding to a total acquisition time of ≈ 10s for the considered number of pixels. Note that due to the time-tagged nature of the data, the acquisition time can be reduced when building the histograms. We analysed the proposed algorithm using the acquisition times of 3.2ms, 1ms, 0.5ms and 0.1ms, where a long acquisition time leads to more detected photons and a better image quality. As explained previously, the proposed algorithm estimates a matrix $\boldsymbol{X}$ whose nonzero elements, higher than a small threshold, provide information about the presence of a target. Therefore, its restoration performance is evaluated through visual inspection of the estimated depth and reflectivity images associated with the actor. These images were estimated by selecting the range's window of $\hat{\boldsymbol{X}}$ after the camouflage, denoted by $\hat{\boldsymbol{X}}_{\text{Man}}$. The man's depth is then estimated as the position of the maximum of each pixel of $\hat{\boldsymbol{X}}_{\text{Man}}$ and the intensity as the sum of photon counts around this maximum (window of 10 bins). These images are compared to those obtained using the maximum likelihood depth solution assuming no background [11, 14], i.e., the classical log-matched filter (denoted by Class.) applied on gated histograms $\boldsymbol{Y}_{\text{Man}}$. It is also compared to the recently proposed approach [4, 22], which assumes an ℓ_1 regularization term, given by

$$g\left(\boldsymbol{X}\right) = \mathcal{L}\left(\boldsymbol{X}\right) + i_{\mathbb{R}_+}\left(\boldsymbol{X}\right) + \lambda_1 ||\boldsymbol{X}||_1 \qquad (13)$$

and has been solved by adapting the ADMM algorithm accordingly. The regularization parameters of (10) and (13) were evaluated at $[10^{-3}, 10^{-2}, 10^{-1}, 1, 10]$, and we only consider the values providing the best visual results. Figs. 2 and 3 show the estimated depth and intensity images with the three algorithms for different acquisition times. It is clear that the performance of all algorithms decreases as the acquisition time is reduced, since the number of photons is reduced. With reduced acquisition time, the classical depth estimates show a higher level of noise while the ℓ_1 based approach presents sparser results. In contrast, the proposed approach offers better restoration results where the noise surrounding the man is reduced and the missing pixels of the part of the image comprising the man are restored. This performance was achieved thanks to the spatial correlation between pixels being considered, and the use of collaborative sparsity to limit the number of active depths which are mainly due to noise. A similar behaviour is observed for the intensities where smoother and less noisy results are obtained by the proposed algorithm, especially at $t = 0.1$ms. These results validate the proposed approach that improves the performance of the sparsity-based single-photon restoration algorithms.

Fig. 1. Observed scene located at 230 m from the scanning system. (Left) Net $\#1$ was placed approximately one meter in front of the actor, (middle) an actor and (right) image of an actor behind camouflage.

5. CONCLUSIONS

This paper has presented a new algorithm to restore the three-dimensional data cube representing histograms of single-photon data. The proposed method is based on an optimization of a convex cost function composed of a data fidelity term and regularization terms. The former term was introduced based on the Poisson statistics of the data. The proposed regularization terms introduced the prior knowledge about the data, namely, (i) the spatial correlation between pixels in small depth regions which was introduced using a total variation regularization term and (ii) the presence of a small number of depths inside the range window whose sparsity effect was promoted using a collaborative sparsity regularization term. The resulting problem was solved using an ADMM algorithm that has good convergence properties. The proposed formulation and algorithm showed good restoration results when processing real images representing a man standing behind a camouflage. Future work includes the generalization of this method to data acquired in corrupting environments such as underwater images.

6. REFERENCES

[1] M.-C. Amann, T. M. Bosch, M. Lescure, R. A. Myllylae, and M. Rioux, "Laser ranging: a critical review of unusual techniques for distance measurement," *Opt. Eng.*, vol. 40, pp. 10–19, Jan. 2001.

ISBN 978-0-9928626-7-1 © EURASIP 2017

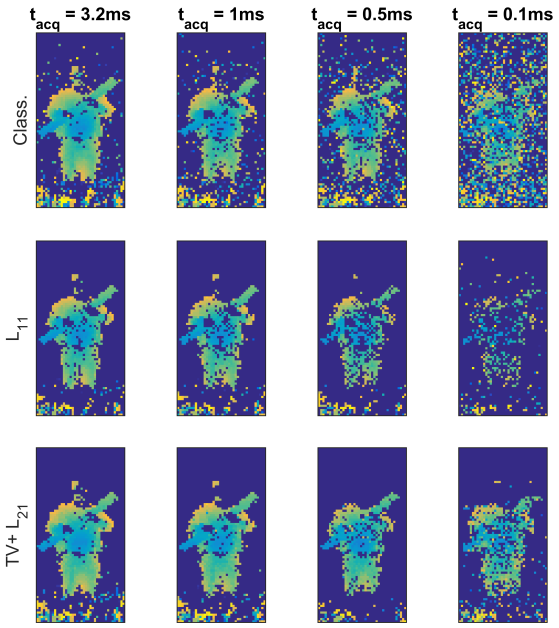

Fig. 2. Depth maps of the man for acquisition time that vary in $(3.2, 1, 0.5, 0.1)$ms, from left to right. From top to bottom, Classical, ℓ_1-based and the proposed TV+ℓ_{12} algorithms. The color scale is [0, 0.54]m for all images.

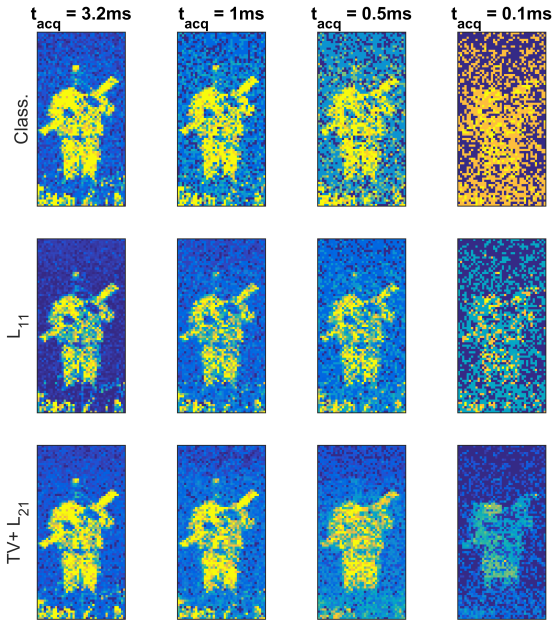

Fig. 3. Intensity maps of the man for acquisition time that vary in $(3.2, 1, 0.5, 0.1)$ms, from left to right. From top to bottom, Classical, ℓ_1-based and the proposed TV+ℓ_{12} algorithms. The color scale is [0, 20], [0, 6], [0, 3], [0, 1] counts, from left to right columns.

[2] G. S. Buller and A. Wallace, "Ranging and three-dimensional imaging using time-correlated single-photon counting and point-by-point acquisition," vol. 13, no. 4, pp. 1006–1015, July 2007.

[3] S. Hernandez-Marin, A. M. Wallace, and G. J. Gibson, "Multilayered 3D lidar image construction using spatial models in a bayesian framework," *IEEE Trans. Pattern Anal. Mach. Intell.*, vol. 30, no. 6, pp. 1028–1040, June 2008.

[4] D. Shin, F. Xu, F. N. C. Wong, J. H. Shapiro, and V. K. Goyal, "Computational multi-depth single-photon imaging," *Opt. Express*, vol. 24, no. 3, pp. 1873–1888, Feb 2016.

[5] L. I. Rudin, S. Osher, and E. Fatemi, "Nonlinear total variation based noise removal algorithms," *Phys. D*, vol. 60, no. 1-4, pp. 259–268, Nov. 1992.

[6] P. Sprechmann, I. Ramirez, G. Sapiro, and Y. C. Eldar, "C-Hilasso: A collaborative hierarchical sparse modeling framework," *IEEE Trans. Signal Process.*, vol. 59, no. 9, pp. 4183–4198, Sept 2011.

[7] H. K. Aggarwal and A. Majumdar, "Hyperspectral unmixing in the presence of mixed noise using joint-sparsity and total variation," *IEEE J. Sel. Topics Appl. Earth Observat. Remote Sens.*, 2016, to appear.

[8] M. D. Iordache, J. M. Bioucas-Dias, and A. Plaza, "Collaborative sparse regression for hyperspectral unmixing," *IEEE Trans. Geosci. Remote Sens.*, vol. 52, no. 1, pp. 341–354, Jan 2014.

[9] S. Boyd, N. Parikh, E. Chu, B. Peleato, and J. Eckstein, "Distributed optimization and statistical learning via the alternating direction method of multipliers," *Found. Trends Mach. Learn.*, vol. 3, no. 1, pp. 1–122, Jan 2011.

[10] M. Figueiredo and J. Bioucas-Dias, "Restoration of Poissonian images using alternating direction optimization," *IEEE Trans. Image Process.*, vol. 19, no. 12, pp. 3133–3145, Dec 2010.

[11] A. Halimi, Y. Altmann, A. McCarthy, X. Ren, R. Tobin, G. S. Buller, and S. McLaughlin, "Restoration of intensity and depth images constructed using sparse single-photon data," in *Proc. EUSIPCO*, 2016, pp. 86–90.

[12] M.-D. Iordache, J. Bioucas-Dias, and A. Plaza, "Total variation spatial regularization for sparse hyperspectral unmixing," *IEEE Trans. Geosci. Remote Sens.*, vol. 50, no. 11, pp. 4484–4502, Nov. 2012.

[13] S. Hernandez-Marin, A. Wallace, and G. Gibson, "Bayesian analysis of Lidar signals with multiple returns," *IEEE Trans. Pattern Anal. Mach. Intell.*, vol. 29, no. 12, pp. 2170–2180, Dec. 2007.

[14] Y. Altmann, X. Ren, A. McCarthy, G. S. Buller, and S. McLaughlin, "Lidar waveform based analysis of depth images constructed using sparse single photon data," *IEEE Trans. Image Process.*, vol. 25, no. 5, pp. 1935–1946, Mar. 2015.

[15] N. Komodakis and J. C. Pesquet, "Playing with duality: An overview of recent primal?dual approaches for solving large-scale optimization problems," *IEEE Signal Processing Magazine*, vol. 32, no. 6, pp. 31–54, Nov 2015.

[16] M. Afonso, J. Bioucas-Dias, and M. Figueiredo, "An augmented lagrangian approach to the constrained optimization formulation of imaging inverse problems," *IEEE Trans. Image Process.*, vol. 20, no. 3, pp. 681–695, March 2011.

[17] J. Eckstein and D. P. Bertsekas, "On the Douglas-Rachford splitting method and the proximal point algorithm for maximal monotone operators," *Math. Programm.*, vol. 55, no. 1, pp. 293–318, 1992.

[18] P. L. Combettes and J.-C. Pesquet, *Proximal Splitting Methods in Signal Processing*. New York, NY: Springer New York, 2011, pp. 185–212.

[19] M. Figueiredo and J. Bioucas-Dias, "Restoration of poissonian images using alternating direction optimization," *IEEE Trans. Image Process.*, vol. 19, no. 12, pp. 3133–3145, Dec 2010.

[20] A. McCarthy, X. Ren, A. D. Frera, N. R. Gemmell, N. J. Krichel, C. Scarcella, A. Ruggeri, A. Tosi, and G. S. Buller, "Kilometer-range depth imaging at 1550 nm wavelength using an InGaAs/InP single-photon avalanche diode detector," *Opt. Express*, vol. 21, no. 19, pp. 22 098–22 113, Sep 2013.

[21] A. M. Wallace, J. Ye, N. Krichel, A. McCarthy, R. Collins, and G. S. Buller, "Full waveform analysis for long-range 3d imaging laser radar," *EURASIP Journal on Advances in Signal Processing*, vol. 2010, no. 1, p. 896708, Dec. 2010.

[22] D. Shin, J. H. Shapiro, and V. K. Goyal, "Computational single-photon depth imaging without transverse regularization," in *Proc. IEEE Int. Conf. Image Process. (ICIP)*, Sept 2016, pp. 973–977.

ISBN 978-0-9928626-7-1 © EURASIP 2017